ADVANCED MATERIALS INTERFACES

Supporting Information

for *Adv. Mater. Interfaces,* DOI: 10.1002/admi.201901805

Semiconducting Metal Oxide Photonic Crystal Plasmonic Photocatalysts

Gillian Collins, Alex Lonergan, David McNulty, Colm Glynn, Darragh Buckley, Changyu Hu, and Colm O'Dwyer**

Supporting Information for

Semiconducting Metal Oxide Photonic Crystal Plasmonic Photocatalysts

Gillian Collins[1,2,3], Alex Lonergan[1], David McNulty[1], Colm Glynn[1], Darragh Buckley[1], Changyu Hu[1], and Colm O'Dwyer[1,2,3,4]

[1] *School of Chemistry, University College Cork, Cork, T12 YN60, Ireland*

[2]*Micro-Nano Systems Centre, Tyndall National Institute, Lee Maltings, Cork, T12 R5CP, Ireland*

[3]*AMBER@CRANN, Trinity College Dublin, Dublin 2, Ireland*

[4]*Environmental Research Institute, University College Cork, Lee Road, Cork T23 XE10, Ireland*

Additional materials characterisation

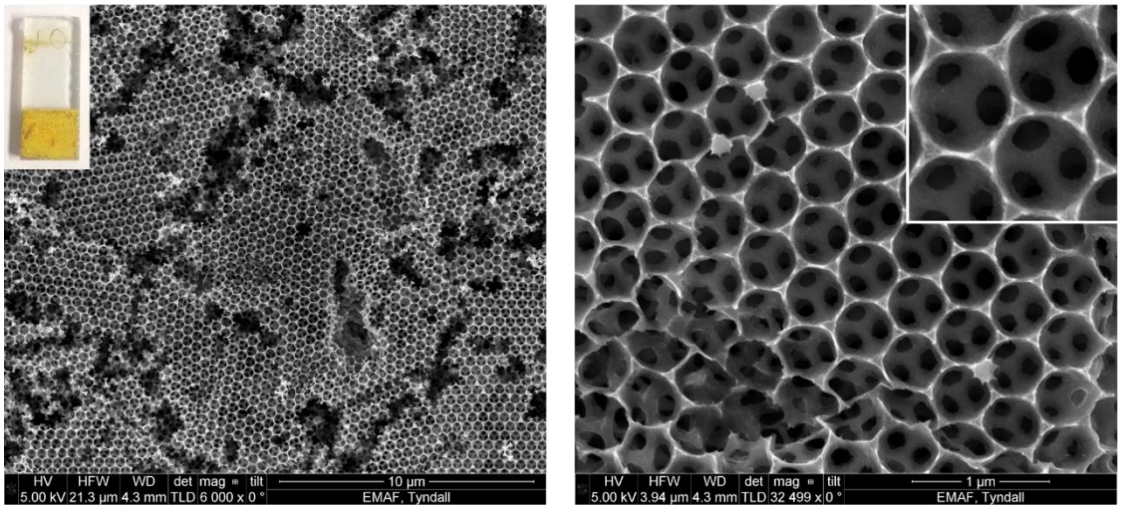

Figure S1. Scanning electron microscopy images of a typical V_2O_5 IO. Inset is a photograph of an IO film on FTO-coated glass.

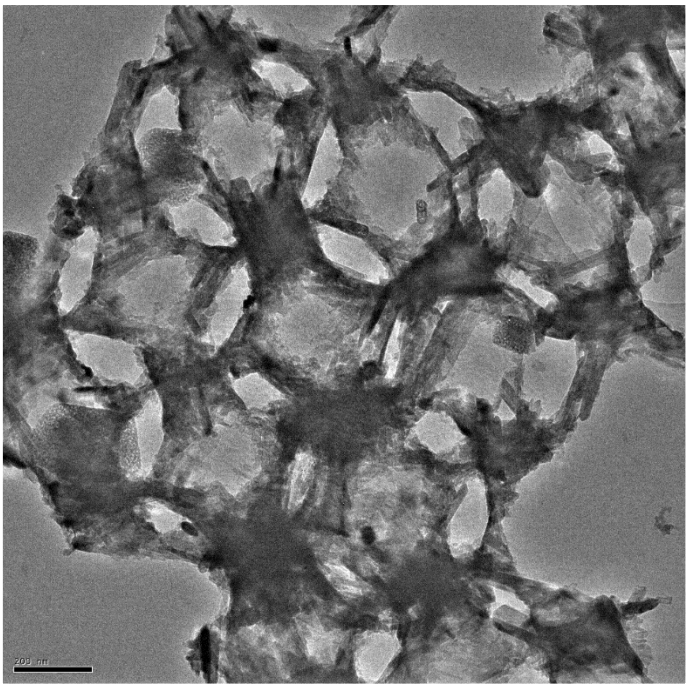

Figure S2. Transmission electron microscopy image of a section of V_2O_5 IO. Tetrahedral and octahedral infilled regions, and the pore walls that define the IO structure in two layer are visible in projection. As V_2O_5 is an orthorhombic crystal structure with a layered morphology, the walls are characteristically rougher compared to TiO_2, which maintains a nanoparticulate wall texture.

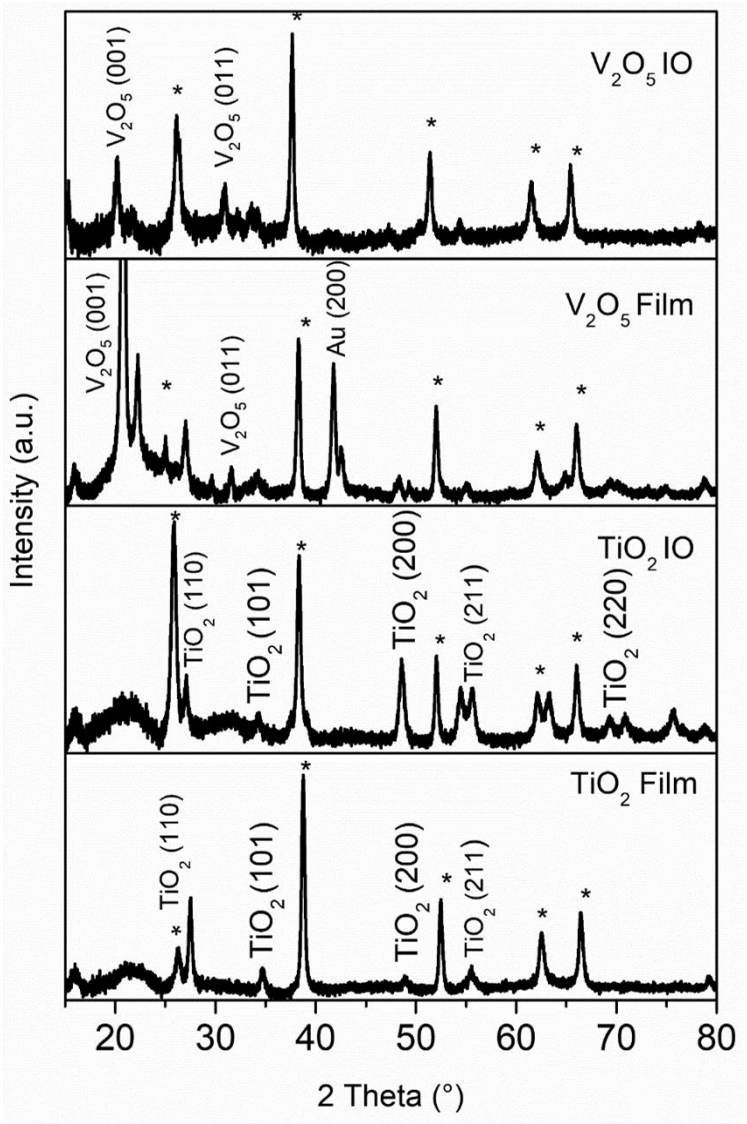

Figure S3. XRD patterns of V_2O_5 and TiO_2 IO and non-porous thin films on FTO. Reflections (*) are from the underlying FTO-coated glass substrate. The Au(200) reflection originates from the semi-transparent gold coating sample preparation used for SEM imaging of the thin film.

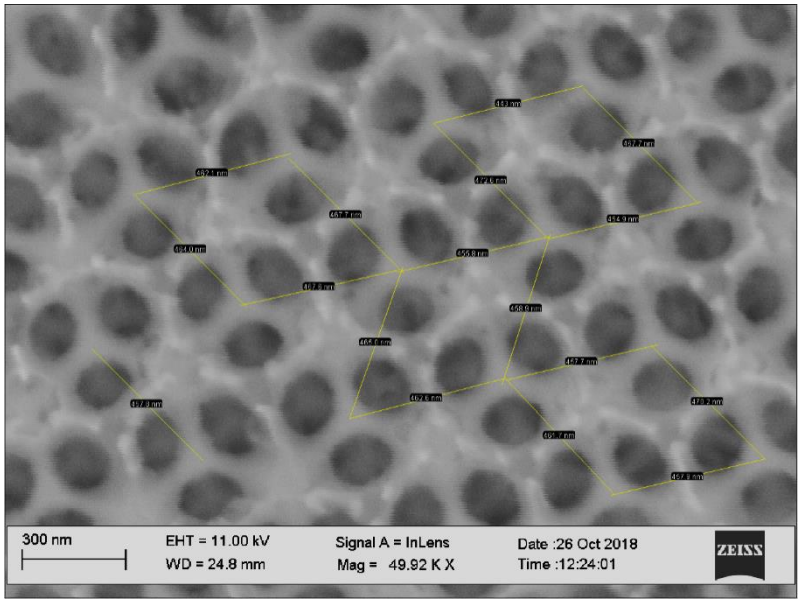

Figure S4. Scanning electron microscopy image a typical V_2O_5 IO. As the IO is formed from an opal template using 500 nm diameter PS spheres, the resulting IO periodicity ranges from 450-470 nm.

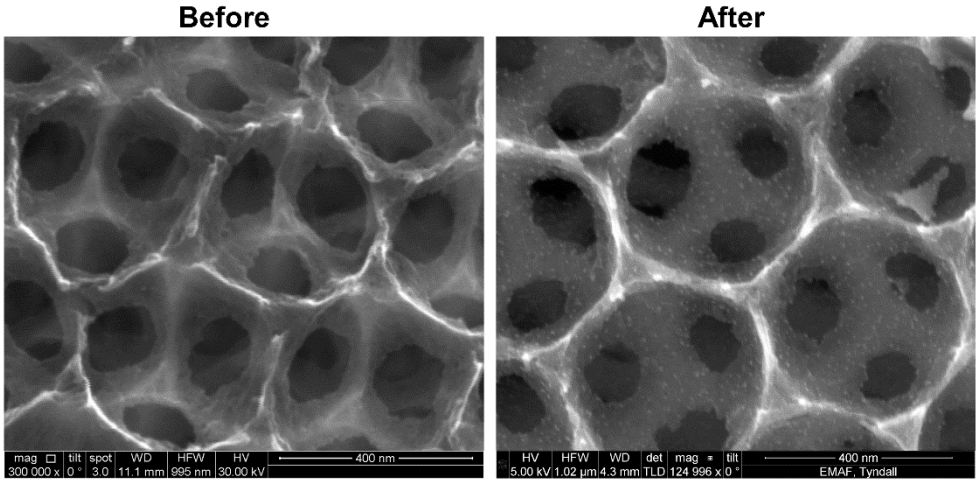

Figure S5. Scanning electron microscopy images of a V_2O_5 IO before and after Au NP surface functionalization.

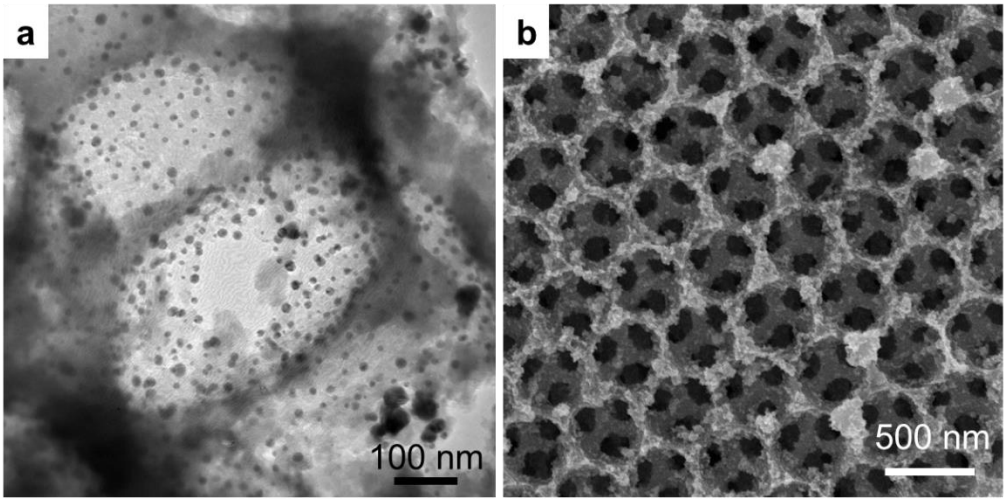

Figure S6 (a) Transmission electron microscopy image and (b) scanning electron microscopy image of 15 nm citrate stabilized Au nanoparticles on TiO_2 IO.

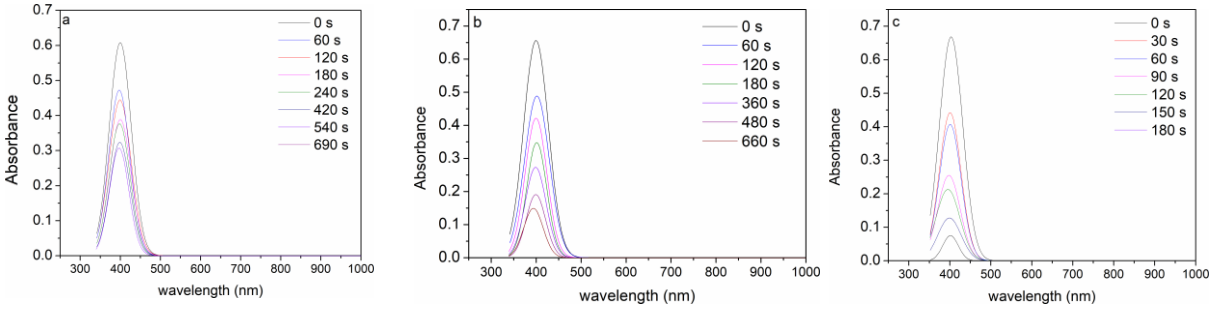

Figure S7. UV-vis absorbance spectra of the photocatalytic reduction of 4-nitrophenol (4-NP) (a) in the dark, (b) under broadband white light illumination and (c) illuminated with green laser light (λ = 532 nm).

Light transmission through inverse opal photonic crystals

For straight through optical transmission, spectra were acquired using broadband white light and intensity background from FTO-coated glass was subtracted. In addition, angle-resolved measurements of TiO_2 and V_2O_5 IO shown in Fig. S8 were acquired to determine the consistency of the pseudo photonic bandgap. The measurements confirmed the stop band and transmission dip varied with angle as expected from Bragg-Snell law and associated dispersion relations.

From the Bragg-Snell relation, the transmission minimum is usually defined by $\lambda_{hkl} = \frac{2d_{hkl}}{m}\sqrt{{n_{avg}}^2 - sin^2\theta}$ for an FCC lattice, and angle resolved dependence can be described according to $\lambda_{hkl} = \frac{2d_{hkl}}{m}\sqrt{{n_{avg}}^2 - sin^2\theta}$ for the IO with air-filled pores. The transmission spectra are shown in Fig. S7 and the Bragg-Snell plot of the shift in transmission minimum (PBG) with angle is also shown.

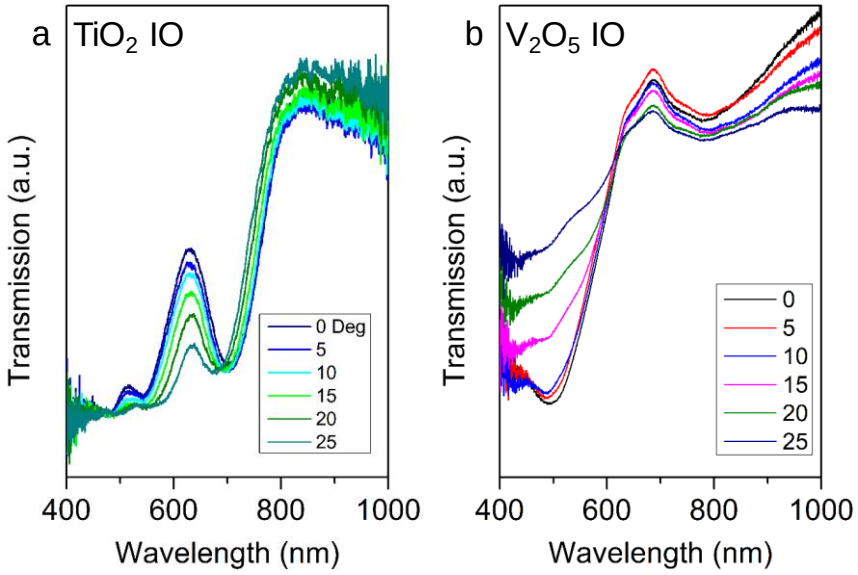

Figure S8. Angle-resolved optical transmission spectra for (a) TiO_2 IOs fashioned from infilling of an opal comprising 500 nm PS spheres, and (b) the corresponding V_2O_5 IO.

In these calculations, we use our recent modification to the standard theory for the angle-resolved spectral analysis of periodic inverse opal structures, namely that the dimension $d_{hkl} = \frac{1}{\sqrt{3}} D$. This arises from consideration of the geometric structure that interact with incident light, defining a periodic inverse opal unit cells formed from interstitial tetrahedral sites with reduced unit cell parameter of length D and from interstitial octahedral sites with standard unit cell parameter of length $\sqrt{2}\,D$. Thus, the transmission dip is the spectra of TiO_2 IO and V_2O_5 IO are consistent with the pseudo PBG defined with solvent-filled pores according to $\lambda_{hkl}{}^2 = 4{d_{hkl}}^2 n_{avg}^2 - 4{d_{hkl}}^2 n_{sol}^2 \frac{n_{avg}^2}{n_{sub}^2} \sin^2\theta$, and we can thus define it's spectral location compared to the materials electronic band edge and that LSPR of the surface-immobilized Au NPs.

Finite difference time domain model details

Periodical IO structures can be characterized as discrete periodic changes of $\varepsilon(r)$. The method acts on photons which is analogous to the way an atomic crystalline potential acts on electrons: the discrete periodicity of $\varepsilon(r)$ in one direction that results in a dependence of $\boldsymbol{H}(\boldsymbol{r})$ in that direction which is a plane wave modulated with a function $u_k^{(r)}$ that has the periodicity of the lattice, to give the Bloch state:

$$H_r(k) = e^{i(k \cdot r)} \cdot u_k^{(r)}$$

where $\boldsymbol{k}$ is the wavevector. For each respective $\boldsymbol{k}$, we compute the corresponding band index n as a series of eigenmodes with discretely spaced frequencies. The band diagram or dispersion curve can be calculated, as each $\omega_n(k)$ changes continuously with $\boldsymbol{k}$. In Fig. S8, a numerical calculation schematic of IO photonic crystal is presented. The FDTD model

used 2D slabs with the same FCC packing structure to model the inverse opal in the electrolyte used during photocatalytic experiments. The pores were assumed to be completed electrolyte filled and the nominal refractive indices are summarised in the table below. The periodicity of IO is set as 420 nm, and the radius of IO pore is 380 nm. The refractive index of TiO_2 and V_2O_5 are 2.6 and 1.8 in the solvent with 1.45, respectively [1].

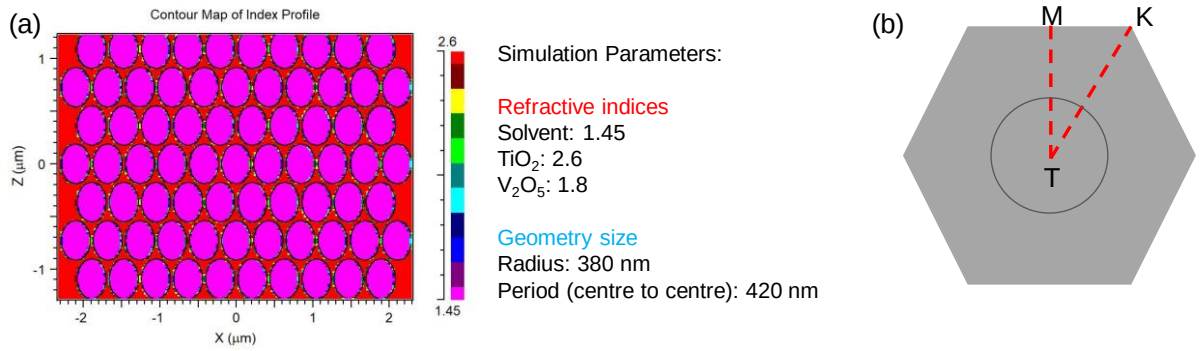

Figure S9. FDTD 2D simulation schematic and parameter settings are presented in (a), with a corresponding first Brillouin zone shown in (b).

Using the eigenfrequency numerical calculation, we started by calculating the eigenfrequencies at $\boldsymbol{k}$ = 0, and use them as the initial inputs to iterative compute eigenmodes for small increments of $\boldsymbol{k}$. Thus, the resulting photonic band structures for TiO_2 and V_2O_5 IO are as follows:

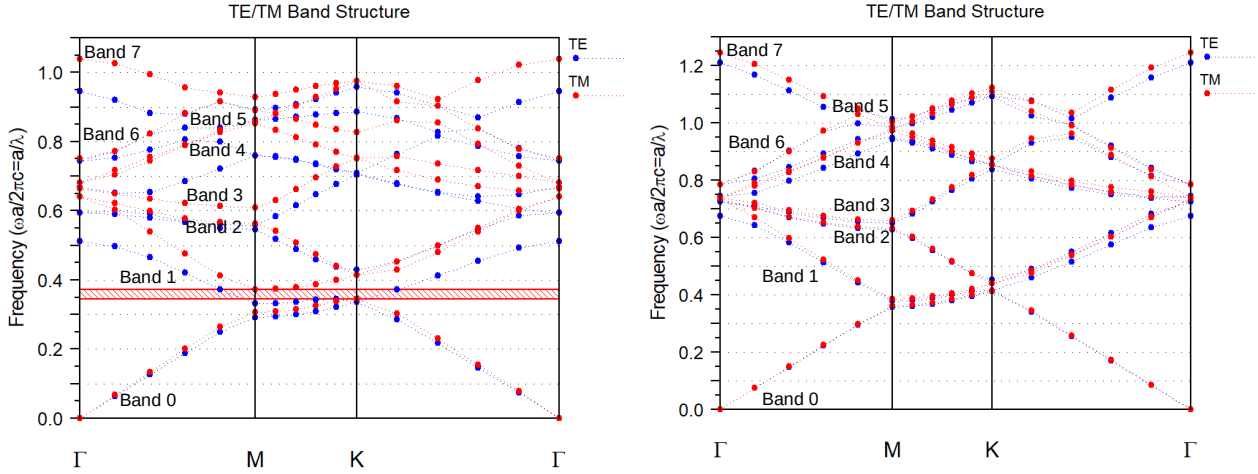

Figure S10. Photonic band structures of TiO_2 (left) and V_2O_5 (right) inverse opal photonic crystals by FDTD calculations in TE and TM polarizations. Red shadow region shows a band gap over the full direction.

From these, we calculated both dispersion and group index (see main text) as a function of wavelength to isolate and compare the spectra range and relative influence of slow photons caused by higher photon group velocities.

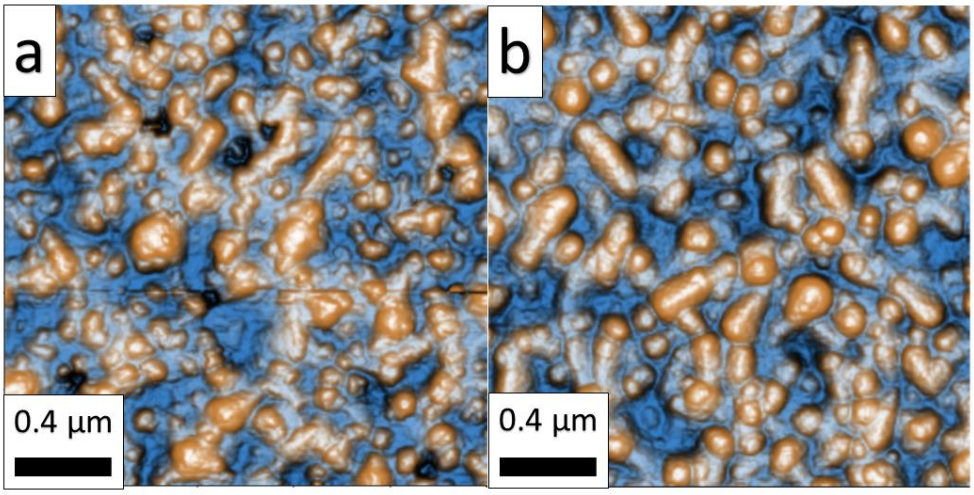

Figure S11. Atomic force microscopy images acquired using intermittent contact mode of the (a) V_2O_5 and (b) TiO_2 thin films surfaces.

[1] J. R. Devore, Refractive indices of rutile and sphalerite, J. Opt. Soc. Am. 41, 416-419 (1951)